

## High-performance double-filter soft x-ray diagnostic for measurement of electron temperature structure and dynamics

M. B. McGarry, P. Franz, D. J. Den Hartog, J. A. Goetz, M. A. Thomas et al.

Citation: *Rev. Sci. Instrum.* **83**, 10E129 (2012); doi: 10.1063/1.4740274

View online: <http://dx.doi.org/10.1063/1.4740274>

View Table of Contents: <http://rsi.aip.org/resource/1/RSINAK/v83/i10>

Published by the [American Institute of Physics](http://www.aip.org).

### Additional information on *Rev. Sci. Instrum.*

Journal Homepage: <http://rsi.aip.org>

Journal Information: [http://rsi.aip.org/about/about\\_the\\_journal](http://rsi.aip.org/about/about_the_journal)

Top downloads: [http://rsi.aip.org/features/most\\_downloaded](http://rsi.aip.org/features/most_downloaded)

Information for Authors: <http://rsi.aip.org/authors>

## ADVERTISEMENT

**physicstoday**

Comment on any  
*Physics Today* article.

Physics Today / Volume 63 / Issue 7 / July 2012  
Previous Article | Next Article

**Measured energy in Japan**  
David von Seggern  
([rvseg@seismo.unr.edu](mailto:rvseg@seismo.unr.edu)) University of Nevada  
July 2012, page 10  
DIGITAL OBJECT IDENTIFIER  
<http://dx.doi.org/10.1063/PT.3.1619>

The article by Thorne Lay and Hiroo Kanamori (10E129) is an excellent review of the seismic energy release from the 1964 Chilean earthquake. The authors used the relation for seismic energy release rather than total strain energy release. The seismic energy underestimates the total strain energy release by a factor of about 3, or 15 times if one accounts for the energy released in the aftershock sequence. The seismic energy underestimates the total strain energy release by a factor of about 3, or 15 times if one accounts for the energy released in the aftershock sequence. The seismic energy underestimates the total strain energy release by a factor of about 3, or 15 times if one accounts for the energy released in the aftershock sequence.

**Comment on this article**  
By the act of hitting a ball with a bat, one calculates the force energy to deliver the ball to its new location, but one must also take into account that the ball extended its energy to the strike team, which became struck by the ball as its momentum ceased and passed energy to the strike team. Therefore the parameters of the damage extend into the future when the received energy to that pushed upon, later becomes released in a new event. Perhaps calculations of one added that in, while another's calculations did not. E.M.C.  
Written by Edgar Mocarvill, 14 July 2012 19:59

# High-performance double-filter soft x-ray diagnostic for measurement of electron temperature structure and dynamics<sup>a)</sup>

M. B. McGarry,<sup>1,b)</sup> P. Franz,<sup>2</sup> D. J. Den Hartog,<sup>1</sup> J. A. Goetz,<sup>1</sup> M. A. Thomas,<sup>1</sup> M. Reyfman,<sup>1</sup> and S. T. A. Kumar<sup>1</sup>

<sup>1</sup>*Department of Physics, University of Wisconsin-Madison, Madison, Wisconsin 53706, USA*

<sup>2</sup>*Consorzio RFX, Associazione Euratom-ENEA per la Fusione, Padova, Italy*

(Presented 9 May 2012; received 4 May 2012; accepted 17 July 2012; published online 7 August 2012)

A new soft x-ray (SXR)  $T_e$  and tomography diagnostic has been developed for MST that can be used for simultaneous SXR spectrum measurement, tomographically reconstructed emissivity, and reconstructed and line-of-sight electron temperature. The diagnostic utilizes high-performance differential transimpedance amplifiers (gain  $10^5$ – $10^9$ ) to provide fast time response (up to 125 kHz), allowing for the study of plasma structure dynamics. SXR double-foil  $T_e$  measurements are consistent with Thomson scattering. SXR brightness through a variety of filter thicknesses has been combined with charge exchange recombination spectroscopy (CHERS) impurity density measurements to determine the plasma energy spectrum. Magnetic pickup from the fluctuating magnetic fields in the plasma ( $\tilde{B} \sim 20$  gauss at 10–20 kHz) has been dramatically reduced by improving the detector and housing design, so that nanoampere diode currents are now measured without interference from the substantial fluctuating magnetic field incident on the plasma facing surface of the probe. © 2012 American Institute of Physics. [<http://dx.doi.org/10.1063/1.4740274>]

## I. INTRODUCTION

Soft x-ray (SXR) bremsstrahlung brightness measurements have been tomographically reconstructed into emissivity maps, for example on the MST and RFX reversed field pinch experiments, to study the evolution of magnetic islands.<sup>1–3</sup> Moreover, the double-foil ratio technique can be applied to brightness or emissivity measurements to calculate electron temperature ( $T_e$ ).<sup>4</sup> The double-foil technique has been used on RFX and NSTX for single-point and radial  $T_e$  profile measurements.<sup>5–7</sup>

A SXR diagnostic has been developed for MST that provides multiple SXR measurement capabilities in a single instrument by combining four detectors at different poloidal angles for tomographic reconstruction of emissivity with pairs of sight-lines sharing two different beryllium filters for double-foil temperature measurements.<sup>8</sup> Additionally, the double-foil technique applied to reconstructed emissivities generates a 2D poloidal map of  $T_e$ . A previous SXR diagnostic on MST made tomographic measurements of emissivity, but reconstructed  $T_e$  measurements were limited by the diagnostic geometry.<sup>9,10</sup> Finally, the new double-foil diagnostic is capable of determining the gross features of the SXR spectrum. The diagnostic has fast time response (up to 125 kHz), and average chord separation of  $\sim 10$  cm, facilitating the study of plasma structure dynamics.

This paper describes results from commissioning the first detector in the new SXR  $T_e$  and tomography diagnostic. Section II describes the first full diameter profile  $T_e$  measure-

ment on MST and validates the direct-brightness technique by comparing with Thomson scattering  $T_e$ . Section III presents a method to, for the first time, measure the energy spectrum of the plasma by combining the SXR brightness with impurity density measurements from the CHERS diagnostic. Finally, Sec. IV identifies a sensitivity to magnetic pickup that resulted from the new, low-noise performance of the diagnostic's fully differential architecture and describes the thick-walled tellurium copper housing required to successfully shield it out at amplifications up to  $10^8$ .

## II. PROFILE $T_e$ MEASUREMENT

Full diameter  $T_e$  profiles during high-current improved confinement plasmas are measured for the first time using a single prototype SXR detector. The prototype detector is a fan of 10 unique lines-of-sight centered at the magnetic axis, with pairs of detectors looking at each chord through 408  $\mu\text{m}$  and 800  $\mu\text{m}$  Be foils. The diagnostic is located  $22^\circ$  below the midplane and points toward the magnetic axis, generating a nearly vertical profile measurement in the poloidal plane. Figure 1 plots the temperature as a function of normalized impact parameter ( $p$ ), the minimum distance from the chord to the magnetic center of MST, where negative impact parameter is below the midplane. The data have been averaged over a 0.5 ms window to provide an equilibrium profile.

The temperature is calculated using the  $T_e(R)$  equation, which relates the ratio of two filtered signals to the temperature of the plasma assuming bremsstrahlung radiation, and is described in Ref. 11. Uncertainty in the temperature measurement is calculated by propagating the root-mean-square of bandwidth-filtered electronic noise ( $err_f$ ) in the thin and thick filter signals ( $f$ ) through the  $T_e$  calculation using the

<sup>a)</sup>Contributed paper, published as part of the Proceedings of the 19th Topical Conference on High-Temperature Plasma Diagnostics, Monterey, California, May 2012.

<sup>b)</sup>Electronic mail: mbmcgarry@wisc.edu.

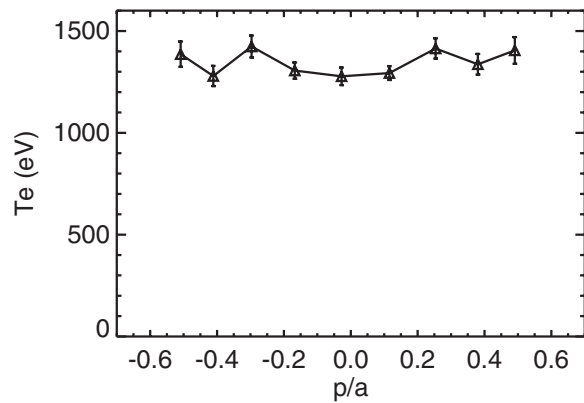


FIG. 1. SXR double-foil  $T_e$  measured from line-integrated brightness as a function of normalized impact parameter during a 500 kA improved confinement plasma. The probe orientation just below the midplane provides a nearly vertical profile measurement, with negative  $p$  below the midplane.  $T_e$  is consistent with Thomson scattering  $T_e$  for a similar shot, shown in Figure 2.

mean of

$$T_{-err} = T_e \left( \frac{f_1 - err_{f_1}}{f_2 + err_{f_2}} \right), \quad T_{+err} = T_e \left( \frac{f_1 + err_{f_1}}{f_2 - err_{f_2}} \right).$$

This error is then combined with a systematic uncertainty in  $T_e$  of  $\sim 2\%$ , arising from uncertainty in filter thickness and numerical variation of the  $T_e$  calculation. Although the Thomson scattering measurement is not currently available for direct comparison, it is possible to compare with similar previous shots. Figure 2 plots  $T_e$  measured using Thomson scattering for another shot also at the time of maximum SXR emission with the same plasma current, reversal parameter, electron density, and magnetic mode activity. Thomson scattering  $T_e$  is plotted against normalized vertical distance below the midplane. Comparison of the two measurements shows good agreement in both amplitude and profile shape. Reconstruction of the magnetic flux surfaces for both shots is planned so that the profiles can be compared directly.

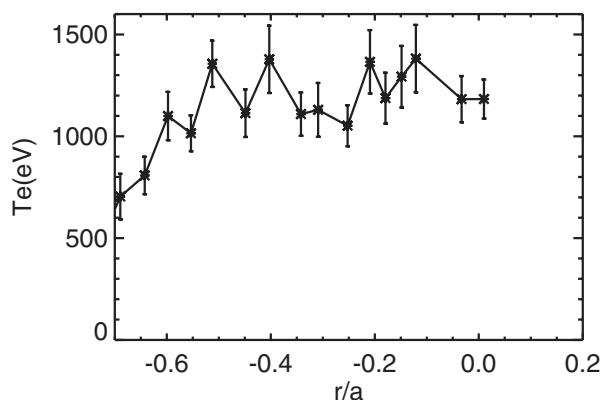


FIG. 2. Thomson scattering  $T_e$  as a function of normalized height below the midplane for a 500 kA improved confinement plasma during peak SXR emission. Although this is a different shot from that shown in Figure 1, the plasma parameters are comparable. Note the coordinate systems in the two plots are not precisely equivalent because the SXR diagnostic is slightly angled with respect to vertical.

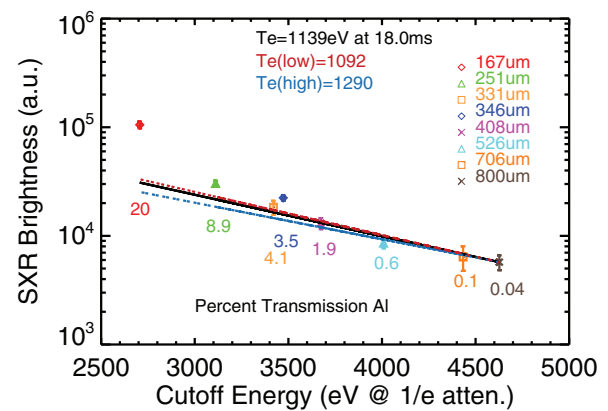


FIG. 3. Energy spectrum as a function of filter  $1/e$  cutoff energy as measured by the SXR  $T_e$  diagnostic. The spectrum combines four similar shots and is representative of a 500 kA improved confinement plasma, with shared plot symbols for filters from the same shot. Shot-to-shot variation in impurity ion density has been normalized using the CHERS  $Al^{11+}$  measurement. For each filter, the percent transmission at 2.3 keV (recombination radiation step) is shown. SXR filters  $< 400 \mu\text{m}$  are susceptible to measuring non-bremsstrahlung contributions.

### III. MEASUREMENT OF THE BREMSSTRAHLUNG ENERGY SPECTRUM

Measurements of SXR brightness through multiple filters are used to determine the SXR energy spectrum of the plasma. The SXR diagnostic measures through two filters in a single shot, so four similar shots are combined for eight filter samples. Figure 3 shows the energy spectrum measured by the SXR diagnostic in the core of MST averaged over 0.5 ms, where the spectrum is normalized for variation in electron density. The CHERS diagnostic measures the  $Al^{11+}$  density for each shot.<sup>12</sup> Al ions are present in the plasma due to the Al walls of the MST vacuum vessel. For the first time, the  $Al^{11+}$  measurement is used to normalize shot-to-shot variation in impurity density as well. The solid line represents the electron temperature measured with the SXR  $T_e$  diagnostic through the thickest pair of foils (408, 800  $\mu\text{m}$ ), assuming pure bremsstrahlung emission. Dashed lines represent uncertainty in  $T_e$ . The number below each point represents the percent transmission through the filter at 2.3 keV (the highest energy aluminum recombination step in the SXR sensitivity range). This provides an indication of the non-bremsstrahlung contribution to the spectrum. For filter thicknesses  $\geq 400 \mu\text{m}$ , non-bremsstrahlung radiation does not affect the spectrum. Using this analysis, an optimal set of Be filters has been selected to minimize Al contamination in the SXR emission measurement.

### IV. DIAGNOSTIC OPTIMIZATION TO REDUCE MAGNETIC PICKUP

When MST is configured so that the reversal surface occurs at the edge of the plasma, the  $n = 5$  magnetic mode becomes dominant and develops a quasi-single helicity structure.<sup>13</sup> Although the mode typically stops rotating when it has saturated, the velocity during the growth phase ranges from 5 to 30 kHz, depending on plasma conditions. This large amplitude oscillating magnetic field can induce a current in

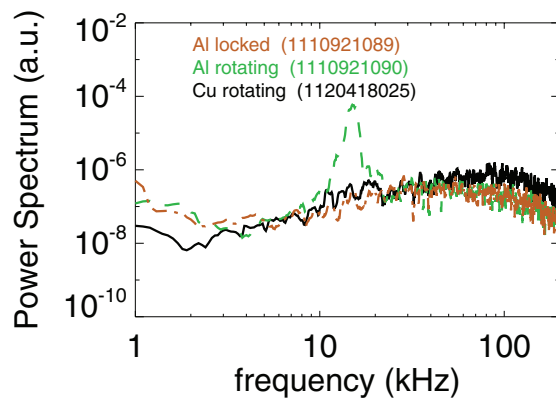


FIG. 4. Power spectra of the non-x-ray contribution for a central diode in the prototype SXR diagnostic. The original thin-walled aluminum design showed magnetic pickup around 15 kHz when the plasma was rotating (dashed green), which disappeared when the plasma locked (dashed-dotted orange). Design improvements, including thick-walled copper housing, now effectively shield out magnetic pickup (solid black).

nearby electronics that are not well shielded. Figure 4 shows the power spectrum of the prototype SXR  $T_e$  and tomography diagnostic for three shots. In all three shots, the diagnostic pinhole is covered (or “blanked”) so that no x-rays can reach the detectors. The first two shots show the impact of magnetic pickup on the original detector design. When the plasma is not rotating (dotted-dashed line), the spectrum is quite flat and reflects the electronic noise floor of the system. However, when the plasma is rotating (dashed line), a peak appears in the spectrum around 15 kHz. This signal has a constant phase relative to a nearby wall-mounted magnetic pickup coil between 12 and 17 kHz, confirming that it is indeed magnetic pickup.

The differential nature of the SXR signals and use of shielded twisted-pair wire eliminate common mode pickup from the external portions of the diagnostic, so two approaches were taken to minimize pickup right at the detectors: the detector board was redesigned to minimize loops of enclosed area, and the probe housing was made out of thick copper to reduce  $\vec{B}$  penetration inside the probe housing. Loops of enclosed area were reduced by a factor of 5 by designing a 5-layer printed circuit board for the diodes and improving the signal cable interface. Additionally, excellent pickup mitigation has been achieved by dramatically increasing the

thickness of the housing wall and changing the material to tellurium copper (C145 alloy). The Cu probe housing has a wall thickness of 4 mm (compared to the original 1.75 mm thick Al walls), and has a 0.25 mm coating of molybdenum on the plasma-facing components to reduce sputtering, leading to  $10^4$  expected reduction in current density on the inner surface of the housing (at 15 kHz).

The third trace in Figure 4 (solid) shows the power spectrum using the new design and amplification  $10^8$  for a similar plasma. In this case, the plasma has an  $n = 5$  dominant mode rotating at 16 kHz during the FFT window. The copper probe data now show no evidence of magnetic pickup. In general, the final design has eliminated measurable pickup for most plasmas at gains of  $10^5$ – $10^8$ . At  $10^9$  gain, pickup is only detected in plasmas with very large rotating magnetic structures, and its amplitude has been dramatically reduced.

<sup>1</sup>R. S. Granetz and P. Smeulders, *Nucl. Fusion* **28**, 457 (1988).

<sup>2</sup>P. Franz, L. Marrelli, P. Piovesan, I. Predebon, F. Bonomo, L. Frassinetti, P. Martin, G. Spizzo, B. E. Chapman, D. Craig, and J. S. Sarff, *Phys. Plasmas* **13**, 012510 (2006).

<sup>3</sup>P. Franz, L. Marrelli, A. Murari, G. Spizzo, and P. Martin, *Nucl. Fusion* **41**, 695 (2001).

<sup>4</sup>F. C. Jahoda, E. M. Little, W. E. Quinn, G. A. Sawyer, and T. F. Stratton, *Phys. Rev.* **119**, 843 (1960).

<sup>5</sup>A. Murari, P. Franz, L. Zabeo, R. Bartiromo, L. Carraro, G. Gadani, L. Marrelli, P. Martin, R. Pasqualotto, and M. Valisa, *Rev. Sci. Instrum.* **70**, 581 (1999).

<sup>6</sup>L. F. Delgado-Aparicio, D. Stutman, K. Tritz, M. Finkenthal, R. Bell, J. Hosea, R. Kaita, B. LeBlanc, L. Roquemore, and J. R. Wilson, *J. Appl. Phys.* **102**, 073304 (2007).

<sup>7</sup>K. Tritz, D. Stutman, L. Delgado-Aparicio, M. Finkenthal, R. Kaita, and L. Roquemore, *Rev. Sci. Instrum.* **81**, 10E502 (2010).

<sup>8</sup>M. B. McGarry, P. Franz, D. J. Den Hartog, and J. A. Goetz, *Rev. Sci. Instrum.* **81**, 10E516 (2010).

<sup>9</sup>P. Franz, F. Bonomo, G. Gadani, L. Marrelli, P. Martin, P. Piovesan, G. Spizzo, B. E. Chapman, and M. Reyfman, *Rev. Sci. Instrum.* **75**, 4013 (2004).

<sup>10</sup>P. Franz, F. Bonomo, L. Marrelli, P. Martin, P. Piovesan, G. Spizzo, B. E. Chapman, D. Craig, D. J. Den Hartog, J. A. Goetz, R. O’Connell, S. C. Prager, M. Reyfman, and J. S. Sarff, *Rev. Sci. Instrum.* **77**, 10 (2006).

<sup>11</sup>P. Martin, A. Murari and L. Marrelli, *Plasma Phys. Controlled Fusion* **38**, 1023 (1996).

<sup>12</sup>S. T. A. Kumar, D. J. Den Hartog, B. E. Chapman, M. O’Mullane, M. Nornberg, D. Craig, S. Eilerman, G. Fiksel, E. Parke, and J. Reusch, *Plasma Phys. Controlled Fusion* **54**, 012002 (2012).

<sup>13</sup>P. Martin, L. Marrelli, A. Alfier, F. Bonomo, D. F. Escande, P. Franz, L. Frassinetti, M. Gobbin, R. Pasqualotto, P. Piovesan, D. Terranova, and RFX-mod Team, *Plasma Phys. Controlled Fusion* **49**, A177 (2007).